Ab initio investigation of the lattice dynamics of fluoride scheelite $LiYF_4$

2005 J. Phys.: Condens. Matter 17 4953

(http://iopscience.iop.org/0953-8984/17/33/001)

INSTITUTE OF PHYSICS PUBLISHING JOURNAL OF PHYSICS: CONDENSED MATTER

J. Phys.: Condens. Matter **17** (2005) 4953–4962 doi:10.1088/0953-8984/17/33/001

Ab initio investigation of the lattice dynamics of fluoride scheelite $LiYF_4$

Benoit Minisini, Qiuping A Wang and François Tsobnang

Institut Supérieur des Matériaux et Mécaniques Avancés du Mans, 44 Avenue Bartholdi, 72000 Le Mans, France

E-mail: bminisini@ismans.univ-lemans.fr

Received 14 April 2005, in final form 28 June 2005
Published 5 August 2005
Online at stacks.iop.org/JPhysCM/17/4953

Abstract

We report on the phonon dynamics of $LiYF_4$ obtained by a direct method using density functional theory. The longitudinal optical/transverse optical (LO/TO) splitting was not investigated. First, the equilibrium structure was evaluated via a full relaxation of the structure. Then phonon dispersion curves, velocities of sound, frequencies of Raman and infrared active modes, and density of states were calculated. Moreover, the elastic stiffness coefficients and specific heat capacity were evaluated from these data. The agreement between calculated and experimental frequencies are acceptable since, in general, the discrepancies are within 8%.

1. Introduction

Research on $LiYF_4$ crystals is strongly linked to laser technology. The first structural data obtained by Thomas *et al* date from 1961 [1], just one year after the demonstration of the first laser. At ambient pressure, the crystal cell of $LiYF_4$ is tetragonal with space group $I4_1/a$ (C_{4h}^6). This phase is commonly named the scheelite structure, in reference to the $CaWO_4$ crystal. the lithium ions (Li^+) are in the centre of tetrahedra composed of four fluoride ions (F^-). The yttrium ions (Y^{3+}) are in the centre of polyhedra composed of eight F^-. Y^{3+} can be substituted by rare earth metals presenting an oxidation state of +3, such as erbium (Er^{+3}) [2] or thulium (Tm^{+3}) [3], providing a good matrix for an up-conversion laser. The efficiency of this kind of laser relies on intraionic and interionic processes of relaxation that strongly depend on the host matrix [4]. Consequently, a fair knowledge of the structural and dynamics properties of the host matrix is crucial for the development of laser materials.

To this end many studies have been carried out on the subject. Phonon frequencies were measured by Raman and infrared spectra [5–9]. Phonon dispersion curves, essential to a good understanding of the global vibrational properties, were obtained by Salaün *et al* [10] using inelastic neutron scattering.

Besides experimental work, numerical methods have been applied. Among them we can notice empirical methods, such as rigid ion model (RIM). Using this method, Salaün *et al* [10] and Sen *et al* [11] performed lattice dynamical calculations on $LiYF_4$. However, the correctness and precision of this model are limited by the empirical parameters.

Density functional theory (DFT) is a method free of structure-dependent parameters whose usefulness and predictive ability in different fields [12, 13] have been known for a long time. Recently, the application of DFT to different techniques such as the linear response method [14, 15] or direct methods [16, 17] have allowed the evaluation of phonon dispersion curves. In particular Parlinski *et al* [18, 19] developed a direct method where the force constant matrices can be evaluated via the Hellmann–Feynman theorem from DFT total energy calculations.

In this work we present a first-principle investigation of $LiYF_4$ in its scheelite phase. DFT associated with the projector augmented wave (PAW) and a direct method were used. Cell parameters, the phonon dispersion curve, and the phonon density of state (DOS) are discussed and compared with previous experimental or numerical results. Sound velocities were extracted from acoustic branches and used to evaluate the elastic constants. To our knowledge, this is the first *ab initio* calculation of $LiYF_4$ lattice dynamics.

2. Methodology

All calculations were carried out with the VASP [20] code, based on DFT [21, 22], as implemented within MEDEA[1] interface. Here the generalized gradient approximation (GGA) through the Perdew Wang 91 (PW91) [23] functional and projector augmented wave (PAW) [24] were employed for all calculations.

The initial model was built from experimental results obtained by Garcia and Ryan [25]. Then, the crystal structure was fully optimized without constraints imposed by the space group symmetry at 0 GPa until the maximum force acting on each atom dropped below 0.002 eV $Å^{-1}$. The self-consistent field (SCF) convergence criterion was set at 10^{-6} eV. High-precision calculations, as defined in VASP terminology, were performed with a basis set of plane waves truncated at a kinetic energy of 700 eV. The Pulay stress [26] obtained on the unit cell was -4 MPa and the convergence of the total energy was within 0.4 meV/atom, compared to an energy of 750 eV. Brillouin zone integrations were performed by using a $3 \times 3 \times 3$ k-points Monkorst–Pack [27] grid leading to a convergence of the total energy within 0.1 meV/cell, compared to a $7 \times 7 \times 3$ k-point mesh.

PHONON code [17], based on the harmonic approximation, as implemented within MEDEA (see footnote 1) was used to calculate the phonon dispersion. From the optimized crystal structure, a $2 \times 2 \times 1$ supercell, consisting of 96 atoms, was generated from the conventional cell to account for an interaction range of about 10 Å. The asymmetric atoms were displaced by ± 0.03 Å leading to 14 new structures. The dynamical matrix was obtained from the forces calculated via the Hellmann–Feynman theorem. Γ point and medium precision, as defined in VASP terminology, were used for these calculations. The error on the force can perturb the translational and the rotational invariance conditions. Consequently, this condition has to be enforced. The strength of enforcement of the translational invariance condition was fixed at 0.1 during the derivation of all force constants. The longitudinal optical (LO) and transverse optical mode (TO) splitting was not investigated in this work. Consequently, only TO modes at the Γ point were obtained.

[1] Materials Design Angel Fire NM.

Table 1. Comparison between calculated at 0 K, experimental, and previously calculated structural parameters of the scheelite $LiYF_4$ structure.

		Experimental results			Numerical results			
	Our work	Ref. [29]	Ref. [30]	Ref. [31]	Ref. [32][a]	Ref. [32][b]	Ref. [33][c]	Ref. [11][d]
a, b (Å)	5.23	5.171	5.16	5.26	5.2	5.08	5.14	5.12
c (Å)	10.82	10.748	10.74	10.94	10.85	10.54	10.82	10.67
c/a	2.07	2.08	2.08	2.08	2.09	2.07	2.11	2.08
Density (Mg m^{-3})	3.86	3.98	4.00	3.78	3.89	4.20	4.00	4.09

[a] DFT/PAW/GGA.
[b] DFT/PAW/LDA.
[c] DFT/OLCAO/LDA.
[d] RIM.

3. Results and discussion

3.1. Structural parameters

Table 1 shows calculated and previous experimental or numerical structural properties of $LiYF_4$. Compared to the most recent experimental data [29, 30], our calculated volume is overestimated. Nevertheless, the c/a axial ratio, whose evolution is significant in the pressure-induced transition phase, is close to experimental results.

DFT results are strongly dependent on the approximation of the exchange correlation term. It is known that the local density approximation (LDA) favours high electron densities, resulting in the prediction of short bonds and hence low equilibrium volume. Results obtained by Li *et al* [32] and Ching *et al* [33] using the LDA illustrate this behaviour. The GGA corrects and sometimes over-corrects the failures of the LDA. That is why the cell parameters obtained using PW91 differ from experimental results. At least two reasons explain why our results are at variance with those of Li *et al* [32]. The first is due to the utilization of different parameters such as the energy cut-off. The other can be attributed to the difference of method to evaluate the equilibrium volume. Indeed, during a structure optimization the convergence criterion is set on the stress. Consequently, the lattice constants are obtained from a cell at its minimum of stress. But a minimum of stress does not mean a minimum of energy. Lattice constants from a cell at its minimum of energy, as performed by Li *et al* [32], are derived through fitting of an energy versus volume curve.

The conventional cell contains 16 fluorine (18.99 g mol^{-1}), 4 lithium (7.01 g mol^{-1}) and 4 yttrium (88.90 g mol^{-1}) atoms. Consequently we obtained a density of 3.86 Mg m^{-3}, which is about 3% lower than the density evaluated from the cell parameters obtained by x-ray diffraction. We can notice that Blanchfield and Saunders [28] measured a floatation density of 3.98 Mg m^{-3}. Bond lengths are presented in table 2. As a result of GGA overcorrection, they are 3% longer than the experimental distances.

3.2. Lattice dynamic

The phonon dispersion curves along several lines of high symmetry for the $LiYF_4$ structure at zero pressure are shown in figure 1. The agreement with experimental data seems acceptable. The main difference concerns the transverse acoustic modes in the **GX** direction. As observed from the RIM calculations [10, 11], a splitting of the longitudinal acoustic branches occurred along the **GX** direction. This splitting is absent from inelastic neutron

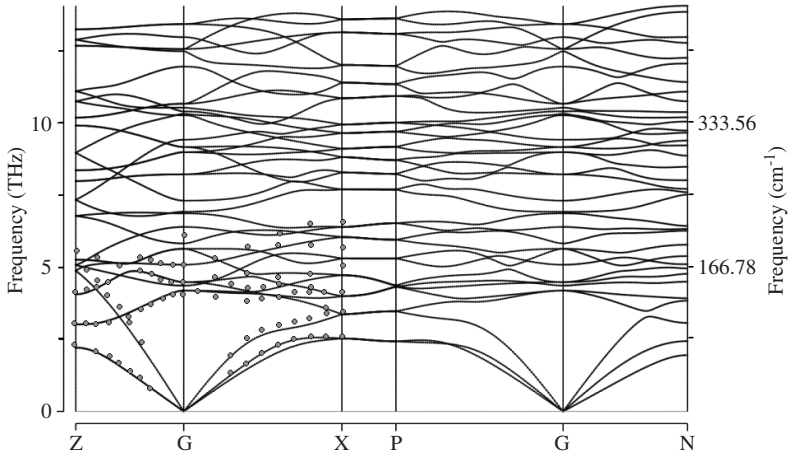

Figure 1. Calculated phonon dispersion (solid line) curves of scheelite $LiYF_4$. Experimental neutron scattering data [11] are denoted by circles. The path is defined in the direction of the quadratic Brillouin zone. The labels are adapted to the symmetry of the active structure. Z (1/2 1/2 −1/2), G = Γ (0 0 0), X (0 0 1/2), P (1/4 1/4 1/4), N (0 0.5 0).

Table 2. Comparison between experimental and calculated interatomic distances.

	Distance (Å)			
		Experimental results		
Ion pair	Our work	Ref. [29]	Ref. [30]	Ref. [31]
Li–F	1.92	1.89	1.89	1.73
Y–F	2.26	2.24	2.24	2.4
Y–F	2.32	2.29	2.29	2.45
F–F	2.62	2.60	2.59	2.71
F–F	2.78	2.75	2.74	2.83
F–F	2.78	2.76	2.76	2.84
F–F	2.86	2.82	2.83	3.03
Li–F	2.93	2.9	2.89	2.96
F–F	2.98	2.95	2.95	3.06

scattering measurements [10] whereas ultrasonic velocities measurements [28] put in evidence the existence of two transverse acoustic modes in this direction.

Velocities of sound along different directions of propagation have been evaluated from the slopes of acoustic branches. Our results at 0 K and experimental ultrasonic velocities at 4.2 K are given in table 3. The difference between calculated and measured velocities lies within 8% for 10 velocities out of 11. However, 20% of the discrepancy is obtained for transverse acoustic branches in the $[0\ 2^{-1/2}\ 2^{-1/2}]$ direction.

As regards the phonon modes, the spectrum contains 36 phonon modes at the **G** point as expected from the number of atoms per primitive cell. From group theoretical considerations, the irreducible representation for the zone centre modes of C_{4h} is given by

$$\Gamma : 3A_g \oplus 5B_g \oplus 5E_g \oplus 5A_u \oplus 3B_u \oplus 5E_u$$

E modes are doubly degenerate, A_g, B_g and E_g modes are Raman active. Four A_u, and four E_u modes are infrared active. One A_u, one E_u and three B_u modes are inactive.

Table 3. Sound velocities in characteristic directions of the propagation vector in the reciprocal lattice.

Direction of propagation vector	Branches		Sound velocities ($m\ s^{-1}$) Calc.	Exp. [28]	Relationships between velocity and elastic constants
[1 0 0]	Longitudinal	v_1	3191	3210	$\rho v_1^2 = C_{44}$
	Transverse	v_2	5673	5510	$\rho v_2^2 = \frac{1}{2}\left\{(C_{11}+C_{66}) + \sqrt{(C_{11}-C_{66})^2+4C_{16}^2}\right\}$
	Transverse	v_3	2127	2068	$\rho v_3^2 = \frac{1}{2}\left\{(C_{11}+C_{66}) - \sqrt{(C_{11}-C_{66})^2+4C_{16}^2}\right\}$
[0 0 1]	Longitudinal	v_4	6319	6240	$\rho v_4^2 = C_{33}$
$[2^{-1/2}\ 2^{-1/2}\ 0]$	Transverse	v_5	5230	5230	$\rho v_5^2 = \frac{1}{2}\left\{(C_{11}+C_{66}) + \sqrt{(C_{12}+C_{66})^2+4C_{16}^2}\right\}$
	Transverse	v_6	2853	2700	$\rho v_6^2 = \frac{1}{2}\left\{(C_{11}+C_{66}) - \sqrt{(C_{12}+C_{66})^2+4C_{16}^2}\right\}$
$[0\ 2^{-1/2}\ 2^{-1/2}]$	Longitudinal	v_7	5569	5840	$\rho(v_7^2+v_8^2+v_9^2) = \frac{1}{2}(C_{11}+C_{66}+C_{33}+3C_{44})$
	Transverse	v_8	3577	3320	$\rho^2(v_7^4+v_8^4+v_9^4) = \frac{1}{4}C_{11}^2+\frac{1}{4}C_{33}^2+\frac{5}{4}C_{44}^2+\frac{1}{4}C_{66}^2$
	Transverse	v_9	2219	2770	$+\frac{1}{2}C_{13}^2+\frac{1}{2}C_{16}^2+\frac{1}{2}C_{44}(C_{11}+C_{66}+C_{33}+2C_{13})$
$[0.5\ 3^{1/2}/2\ 0]$	Transverse	v_{10}	5655	5460	$\rho v_{10}^2 = \frac{1}{2}(C_{11}+C_{66}) + \sqrt{\left[\frac{C_{66}-C_{11}}{2}+\sqrt{3}C_{16}\right]^2+4\left[\frac{\sqrt{3}}{4}(C_{12}+C_{11})-\frac{1}{2}C_{16}\right]^2}$
	Transverse	v_{11}	2219	2210	$\rho v_{11}^2 = \frac{1}{2}(C_{11}+C_{66}) - \sqrt{\left[\frac{C_{66}-C_{11}}{2}+\sqrt{3}C_{16}\right]^2+4\left[\frac{\sqrt{3}}{4}(C_{12}+C_{11})-\frac{1}{2}C_{16}\right]^2}$

The Raman active mode frequencies are presented in table 4. First of all, it should be noticed this calculation was performed at 0 K. The thermal error is not supposed to be very important since, from the results obtained by Raman spectroscopy at 300 and 4.2 K [7], the variation did not exceed 12 cm^{-1}. In general, our calculated frequencies are lower than the experimental results. However, the variation does not exceed 21 cm^{-1} for 10 out of 13 frequencies. The three frequencies showing the highest discrepancy belong to B_g modes with a difference of about 30 cm^{-1}. For the first two modes this difference does not induce a change in the classification. But for the last B_g mode, we can notice a permutation with the fourth E_g mode. This permutation is visible on phonon dispersion curves obtained by Salaün *et al* [10] with the RIM and 11 fitting parameters. But it is absent in the results of Sen *et al* [11] using five variable parameters, showing the dependency of results on the number of variable parameters. The vibration modes are presented in figure 2. The B_g mode calculated at 347 cm^{-1} (the experimental value is 379 cm^{-1} [10]) is mainly due to the translation of the lithium atoms in the direction of the *c*-axis. This movement induces a translation of the fluorine atoms along the direction bridging yttrium and fluorine atoms. The E_g mode calculated at 356 cm^{-1} (the experimental value is 373 cm^{-1} [10]) is mainly due to rotation of the lithium atoms around the *c*-axis. These two mode-dependent movements agree with the symmetry-adapted motions deduced from group theory analysis [5, 6]. We can also notice that the experimental difference between these modes is 6 cm^{-1}, which is very close to the error described by Miller *et al* [6]. It is interesting to notice that the first E_g phonon mode is difficult to measure experimentally because of the polarization effect. This frequency is easily extracted from our results at 149 cm^{-1} (the experimental value is 154 cm^{-1} [5, 8]).

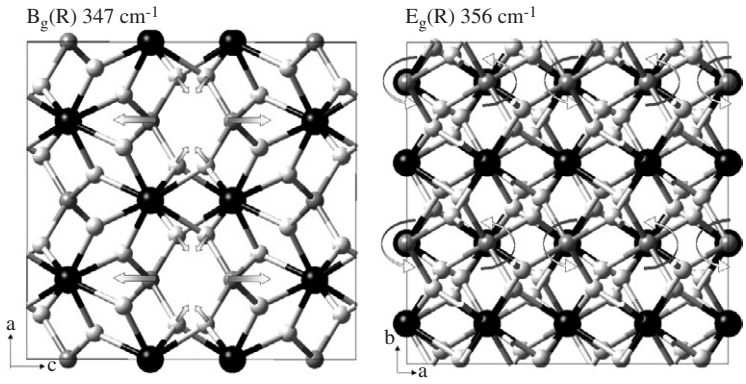

Figure 2. Schematic diagrams of corresponding atomic displacements for the B_g and E_g Raman active modes respectively at 347 and 356 cm^{-1}. Y atoms are represented as black balls, Li atoms are dark grey and F atoms are light grey. the curved arrow means rotation around the *c*-axis.

Table 4. Frequencies of Raman active phonons of scheelite $LiYF_4$.

	Frequencies (cm^{-1})								
		Experimental results						Numerical results[a]	
Phonon symmetry	Our work	Ref. [10][b]	Ref. [8][c]	Ref. [5][c]	Ref. [7][c]	Ref. [6][c]	Ref. [9][c]	Ref. [10]	Ref. [11]
A_g	145	151	151	151	—	—	—	149	151
	244	265	265	265	269	264	261	239	250
	416	427	426	427	426	425	422	419	442
B_g	170	174	173	174	177	177	167	188	174
	213	246	246	246	251	248	241	258	268
	314	327	326	327	331	329	323	319	297
	347	379	379	379	382	382	375	369	391
	398	427	426	427	430	427	423	423	428
E_g	149	154	154	154	158	153	149	152	153
	188	199	198	199	203	199	193	212	207
	306	326	326	326	329	329	322	312	318
	356	373	372	373	376	368	369	378	380
	448	447	446	447	450	446	442	448	449

[a] RIM.
[b] Inelastic neutron scattering.
[c] Raman.

As regards the infrared active modes, as $LiYF_4$ is a weak polar crystal, LO/TO mode splitting is experimentally observed. In our calculation LO/TO mode splitting was not taken into account. Consequently, only infrared TO modes are presented in table 5. From the experimental results obtained at 300 and 77 K [5], it seems that the effect of the temperature induces a small variation; the disparity did not exceed 6 cm^{-1}. In our results obtained at 0 K, four frequencies out of eight are quite close to experimental results obtained by neutron scattering [10]. The difference lies within 3 cm^{-1}. For the other modes the largest discrepancy is 25 cm^{-1}. Three calculated infrared active frequencies are higher than the experimental one, which is more complicated than the situation of Raman modes mentioned above.

Finally, focusing on the classification of the phonon symmetry as a function of their frequencies, we can notice only one permutation below 360 cm^{-1} in comparison with

Table 5. Frequencies of infrared active phonons of scheelite $LiYF_4$.

	Frequencies (cm^{-1})						
		Experimental results				Numerical results[a]	
Phonon symmetry	Our work	Ref. [10][b]	Ref. [5][c]	Ref. [6][d]	Ref. [7][e]	Ref. [10]	Ref. [11]
Au (TO)	194	196	198	195	192	192	199
	231	251	251	252	255	272	251
	342	341	339	396	404	324	316
	351	370	372	490	489	403	403
Eu (TO)	140	137	137	143	144	156	141
	274	294	294	293	262	279	263
	300	325	323	326	314	322	319
	419	418	418	424	413	424	410

[a] RIM.
[b] Inelastic neutron scattering 300 K.
[c] Reflexion IR (300 K).
[d] Adsorption IR (77 K).
[e] Adsorption IR (330 K).

experimental frequencies. Above 360 cm^{-1} in addition of the inversion between the E_g and B_g modes described previously, inversions between Raman and infrared active mode were observed. The first concerns the intercalation of the B_g between the two last A_u modes compare to experimental results. The second concerns the E_u mode whose frequency is higher than the last E_g and B_g. Nevertheless, the agreement between calculated and experimental data is better than with the RIM calculation.

The phonon density of states $g(\omega)$ and partial density of states providing the frequency distribution of normal modes are given in figure 3. As expected from the mass of the different constituents, the density of states (DOS) can be divided into two parts. Y vibrations are dominant between 0 and 250 cm^{-1} and vanish after 417.5 cm^{-1}. We can see that in general there is no preferred direction. An exception can be found around 216 cm^{-1} where the movement along the *c*-axis is privileged. Li vibrations begin at 167 cm^{-1} and are dominant between 250 and 500 cm^{-1}. In the range from 250 to 417.5 cm^{-1}, except between 300 and 350 cm^{-1} where no direction was preferred, the vibrations are along the *c*-axis whereas from 417.5 to 500 cm^{-1} movement is in the *ab* plane. We can notice that F movements lie between 0 and 500 cm^{-1}, implying that they are first correlated with Y and then with Li. Movement implying the three different atom types are situated between 167 and 417.5 cm^{-1}. Compared to the DOS obtained by the RIM, an important difference can be noticed above 250 cm^{-1}. The most striking difference concerns the high frequency. Indeed, the DOS calculated in this work stops at 500 cm^{-1} whereas the DOS calculated with the RIM stops at 550 cm^{-1}, implying Li and F correlated vibrations.

3.3. Thermomechanical properties

Elastic constants were evaluated from sound velocities extracted from the slopes of acoustic branches in different directions. The relationships between the velocities and elastic constants used in this study are presented in table 3 (see [28] for a complete discussion about these relationships). Numerical values of the bulk moduli (B), Young's moduli (E), shear moduli (G) and Poisson's ratio (ν) evaluated using the Voigt relationships are given in table 6. For the elastic constants we can notice an error of 69% for C_{16} and 16% for C_{12}, whereas generally the values lie within 4%. However, C_{16} is not used to evaluate the most important mechanical

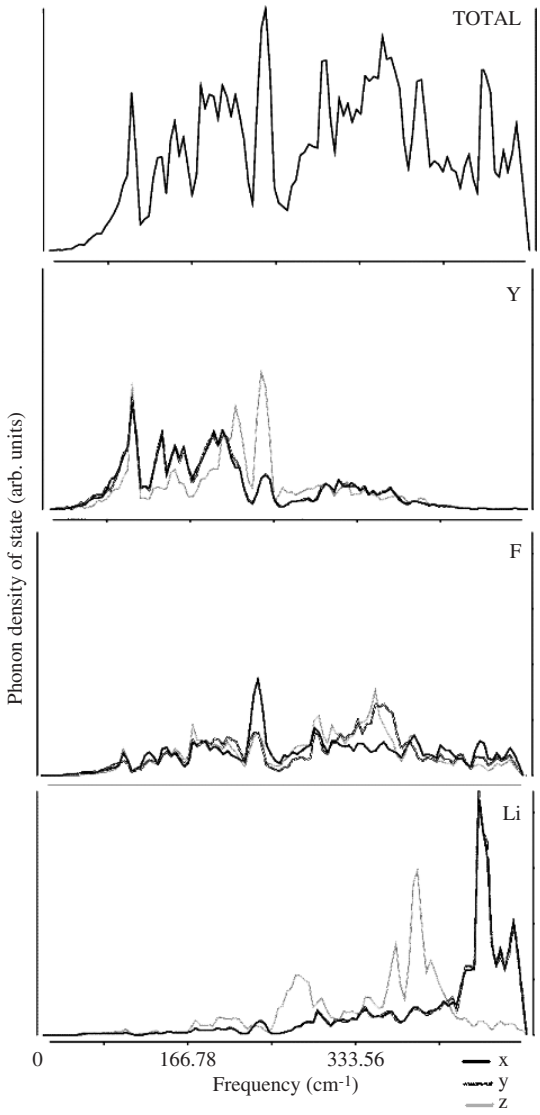

Figure 3. Total and partial phonon density of state calculated for Y, Li and F atoms and x, y, z Cartesian directions.

moduli. That is why an acceptable agreement was found, with a maximum error which does not exceed 4% between calculated and experimental moduli. The bulk modulus is the most extensively studied modulus, providing suitable data for comparison. From fitting with an equation of state, B was evaluated at 80 GPa [34, 35], 94.8 GPa [32] and 69 GPa [36] from experimental, DFT and empirical data respectively. Our result is slightly lower than the experimental one but in better agreement than previous numerical values.

The specific heat capacity at constant volume, C_V, was calculated from the density of states. Within the harmonic approximation, the specific heat capacity at constant pressure, C_P, can be evaluated by the formula

$$C_P = C_V + \beta(T)^2 BVT$$

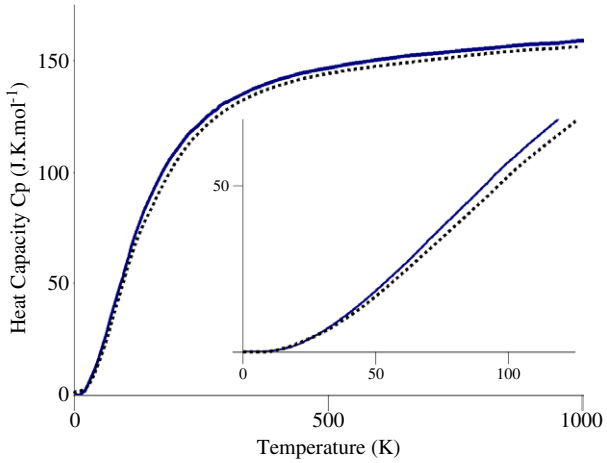

Figure 4. Comparison of specific heat of the $LiYF_4$:RIM results [11] (dashed line) and our DFT results (solid line). The inset details the low-temperature region.

(This figure is in colour only in the electronic version)

Table 6. Elastic stiffness constants and mechanical moduli of scheelite $LiYF_4$. (Note: $G = 1/15(C_{11} + C_{22} + C_{33} - C_{12} - C_{13} - C_{23}) + 1/5(C_{44} + C_{55} + C_{66})$. $B = 1/9(C_{11} + C_{22} + C_{33}) + 2/9(C_{12} + C_{13} + C_{23})$. $\nu = (3B - 2G)/[2(3B + G)]$. $E = (9 * B * G)/(3 * B + G)$.)

	Calc.	Exp. [28]
	Elastic constants	
C_{11}	121	121
C_{12}	51.4	60.9
C_{13}	52.5	52.6
C_{16}	−13	−7.7
C_{33}	153.6	156
C_{44}	39.2	40.6
C_{66}	18.4	17.7
	Modulus	
B bulk (GPa)	79	81
G shear (GPa)	35	35
E Young (GPa)	92	92
ν Poisson	0.305	0.310

where V is the molar volume, $\beta(T)$ the thermal expansion coefficient and B the bulk modulus. Figure 4 represents C_P calculated for an empirical formula of $LiYF_4$ with V obtained after full optimization $V = 44.8\ \text{cm}^3\ \text{mol}^{-1}$, B calculated from the elastic constants obtained from sound velocities extracted from phonon dispersion curves $B = 79$ GPa and $\beta(T)$ was taken to be $\beta(T) = (-4 \times 10^{-5}/T + 1.3/T^2)\sinh^{-2}(149/T)$ [8]. To our knowledge, no experimental data are available for comparison. Compared to the previous numerical study we can notice that our results are slightly higher than values calculated from the RIM.

4. Conclusion

This work presents, to our knowledge, the first *ab initio* lattice dynamics calculation of fluoride scheelite. As regards the phonon dispersion curves, acceptable agreement with inelastic

neutron scattering data was obtained. Discrepancies between sound velocities calculated from acoustic branches and ultrasonic measurement do not exceed 8% for 10 velocities out of 11. Moreover, at the centre of the Brillouin zone the error on Raman active modes calculated compared to experimental results does not exceed 9%, the largest error being 33 cm^{-1}. For the infrared active modes, the error lies within 8%, the largest error being 25 cm^{-1}. Important differences between *ab initio* and RIM calculated DOSs were seen mainly above 500 cm^{-1}. Mechanical properties evaluated from calculated sound velocities are in acceptable agreement compared to experimental values.

Acknowledgments

The authors whish to thank the Materials Design team for numerical support. We express special thanks to Laurent Nivanen for his help in numerical analysis. We are grateful to CCI du Mans et de la Sarthe for providing the calculation infrastructure.

References

[1] Thomas R E, Harris L A, Weaver C F, Friedman H A, Insley H and Yakel H A Jr 1961 *J. Phys. Chem.* **65** 1096
[2] Hubert S, Meichenin D, Zhou B W and Auzel F 1991 *J. Lumin.* **50** 7
[3] Shu Q, Ni H and Rand S C 1997 *Opt. Lett.* **22** 123
[4] Burkhalter R, Dohnke I and Hulliger J 2001 *J. Prog. Cryst. Growth Charact.* **42** 1
[5] Salaün S, Fornoni M T, Bulou A, Rousseau M, Simon P and Gesland J Y 1997 *J. Phys.: Condens. Matter* **9** 6941
[6] Miller S A, Rast H E and Caspers H H 1970 *J. Chem. Phys.* **52** 4172
[7] Schulteiss E, Scharmann A and Schwabe D 1986 *Phys. Status Solidi* b **138** 465
[8] Sarantopoulou E, Raptis Y S, Zouboulis E and Raptis C 1999 *Phys. Rev.* B **59** 4154
[9] Zhang X X, Schulte A and Chai B H T 1994 *Solid State Commun.* **89** 181
[10] Salaün S, Bulou A, Rousseau M, Hennion B and Gesland J Y 1997 *J. Phys.: Condens. Matter* **9** 6957
[11] Sen A, Chaplot S L and Mittal R 2001 *Phys. Rev.* B **64** 024304
[12] Freeman A J and Wimmer E 1995 *Annu. Rev. Mater. Sci.* **25** 7
[13] Matar S F 2003 *Prog. Solid State Chem.* **31** 239
[14] Baroni S, de Gironcoli S and Giannozzi P 1990 *Phys. Rev. Lett.* **65** 84
[15] Baroni S, Giannozzi P and Testa A 1987 *Phys. Rev. Lett.* **58** 1861
[16] Frank W, Elsässer C and Fähnle M 1995 *Phys. Rev. Lett.* **74** 1791
[17] Parlinski K, Li Z Q and Kawazoe Y 1997 *Phys. Rev. Lett.* **78** 4063
[18] Parlinski K and Parlinska-Wojtan M 2002 *Phys. Rev.* B **66** 064307
[19] Parlinski K 2001 *J. Alloys Compounds* **328** 97
[20] Kresse G and Furthmüller J 1996 *Phys. Rev.* B **54** 11169
[21] Hohenberg P and Kohn W 1964 *Phys. Rev.* B **136** 864
[22] Kohn W and Sham L J 1965 *Phys. Rev.* A **140** 1133
[23] Perdew J P, Burke K and Wang Y 1996 *Phys. Rev.* B **54** 16533
[24] Blöchl P E 1994 *Phys Rev.* B **50** 17953
[25] Garcia E and Ryan R R 1993 *Acta Crystallogr.* C **49** 2053
[26] Francis G P and Payne M C 1990 *J. Phys.: Condens. Matter* **2** 4395
[27] Monkhorst H J and Pack J D 1976 *Phys. Rev.* B **13** 5188
[28] Blanchfield P and Saunders G A 1979 *J. Phys. C: Solid State Phys.* **12** 4673
[29] Khajdukov N M, Goryunov A V, Fedorov P P and Popov A I 1992 *Mater. Res. Bull.* **27** 213
[30] Garcia E and Ryan R R 1993 *Acta Crystallogr.* C **49** 2053
[31] Thomas R E, Harris L A, Weaver C F, Friedman H A, Insley H and Yakel H A Jr 1961 *J. Phys. Chem.* **65** 1096
[32] Li S, Ahuja R and Johansson B 2004 *J. Phys.: Condens. Matter* **16** S983–8
[33] Ching W Y and Xu Y N 2001 *Phys. Rev.* B **63** 115101
[34] Blanchfield P, Saunders G A and Hailing T 1982 *J. Phys. C: Solid State Phys.* **15** 2081
[35] Grzechnik A, Syassen K, Loa I, Hanfland M and Gesland J Y 2002 *Phys. Rev.* B **65** 104102
[36] Sen A, Chaplot L S and Mittal R 2002 *J. Phys.: Condens. Matter* **14** 975